ISRN LUTMDN/TMHP-20/5451-SE
ISSN 0282-1990

LUNDS UNIVERSITET

Development of deaeration and oil separation concepts for camless valvetrain auxiliary systems

Daniel Larsson
Emil Ingemansson

Thesis for the degree of Master of Science in Engineering
Division of combustion engines
Department of Energy Sciences
Faculty of Engineering | Lund University

Development of deaeration and oil separation concepts in camless valvetrain auxiliary system

Daniel Larsson
Emil Ingemansson

March 2020, Lund

Föreliggande examensarbete på civilingenjörsnivå har genomförts vid Avd. för Förbränningsmotorer, Inst. för Energivetenskaper, Lunds universitet - LTH samt vid Freevalve i Ängelholm. Handledare på Freevalve: Urban Carlsson; handledare på LTH: Marcus Lundgren; examinator på LTH: Per Tunestål

Projektet har genomförts i samarbete med Freevalve

Examensarbete på Civilingenjörsnivå

ISRN LUTMDN/TMHP-20/5451-SE

ISSN 0282-1990

Avdelningen för Förbränningsmotorer

Institutionen för Energivetenskaper

Lunds Universitet - Lunds Tekniska Högskola

Box 118, 221 00 Lund

www.energy.lth.se

Abstract

Freevalve is a company that is developing a camless valvetrain for use in internal combustion engines. The system, which is operated with the help of a pneumatic system and a hydraulic system working in parallel, can freely control the opening and closure of each individual intake- and exhaust valve.

Oil is used to both cool the air stream in the pneumatic system and to control and dampen the valve motion. The mixing of these medias results in a need to later separate them again to achieve optimal system performance. The purpose of this thesis was to push the development of the oil separation and oil deaeration systems. The focus was therefore to investigate, design and test different concepts for oil separation and deaeration.

Cyclone separators were the main concept further studied regarding oil separation from the air stream, but other non-cyclone designs were evaluated as well. The concepts regarding cyclone separators was evaluated in CFD by looking at the rotational velocity and pressure distribution inside the cyclone chamber. Existing models for cyclone performance and pressure drop were also investigated and used throughout the project. All concepts were thereafter tested practically in a test rig provided by Freevalve. Trends regarding separator efficiencies and flow rates could be established and a design suggestion was presented. The design presented will however need further development until satisfactory performance can be expected across all relevant operating points.

Three deaeration concepts were evaluated but unfortunately with inconclusive results. Mechanisms involved were still studied extensively in order to establish a methodology for solving the issue moving forward and a schematic design was suggested.

Sammanfattning

Freevalve är ett företag som utvecklar ett kamlöst ventilsystem för användning i förbränningsmotorer. Systemet som drivs av ett parallellt pneumatiskt- och hydrauliskt system möjliggör fri och oberoende kontroll av varje insugs- och avgasventil oberoende av varvtal och last.

Olja används både för att kyla luftströmmen samt för att styra ventilrörelsen. Beblandningen av dessa två medierna medför i sin tur ett behov av separering i ett senare skede för att uppnå optimal prestanda i systemet. Syftet med arbetet har varit att driva vidare utvecklingen gällande oljeseparation från luftströmmen samt avluftning av oljan i det hydrauliska systemet. I detta examensarbete fokuseras det därför på att utvärdera och testa olika koncept gällande oljeseparering och avluftning.

Cyklonseparatorer valdes som det huvudsakliga konceptet gällande oljeseparering men även andra typer av koncept undersöktes. Cyklonkoncepten analyserades med hjälp av CFD samt befintliga modeller gällande separeringseffektivitet och tryckförluster. Alla koncept utvärderades därefter praktiskt i en testrigg hos Freevalve. Trender gällande separeringseffektivitet, flödeshastigheter och tryck kunde identifieras och ett designförslag presenterades. Ytterligare arbete anses dock krävas för att tillfredsställande prestanda ska kunna uppnås för fler relevanta driftspunkter.

Tre avluftningskoncept utvärderades vilket inte ledde till att konkreta slutsatser kunde dras kring deras prestanda. Mekanismer gällande avluftning fortsattes studeras noga för att kunna föreslå en framtida lösningsmetodik samtidigt som ett schematiskt designförslag presenterades baserat på litteraturstudien.

Table of contents

Introduction

1.1 Background and Freevalve introduction

Combustion engines have undergone drastic improvements in the last decades, especially when it comes to thermal efficiency. Several things have contributed to this development including increasing fuel prices, emission regulations and automotive marketing from an economic standpoint [1].

One way to increase the efficiency and/or power is to manipulate the intake and exhaust valves in such a way that peak efficiency (or peak power) is reached regardless of the operating point. The camless system from Freevalve that is planned to be implemented for use in future internal combustion engines (ICEs) consists of actuators, solenoids, and control circuits, as well as the parallel pneumatic- and hydraulic auxiliary systems where the focus of this thesis lies, see figure 1.1. The purpose of the pneumatic system is to open and close the valves while the hydraulic system acts to dampen the valve movements and maintain the valves in an open state.

As Freevalves product now moves towards finalisation for implementation in a coming vehicle, a further need for development and packaging of the auxiliary systems was identified.

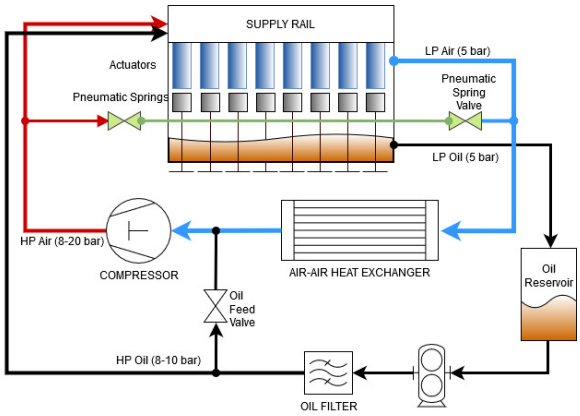

Figure 1.1: Schematic view of Freevalves auxiliary system.

1.2 Problem Formulation and limitations

The main issue regarding separation of oil from the airstream stems from the fact that oil is being injected before the compressor as it acts to cool the compressor when running it at high load, as the performance of the compressor is negatively affected at temperatures over 140°C. Furthermore, the oil acts as a sealant in the compressor which in turn increases its efficiency. This is a problem that has easily been handled in a laboratory setup but becomes more difficult when the system needs to be packageable under the hood of a vehicle. Pressure losses in the system corresponds to overall power losses and reduced efficiency for the system which means that minimising this metric is of importance. As the overall system structure is already put in place, no design changes at this level will be proposed. Instead, separate devices for oil separation and deaeration at the specified load cases and conditions will be investigated and focused on. Inlet and outlet dimensions are also already specified and presented in the system requirements below.

The air after the compressor contains at most 1,5 - 2,0% oil (in volume), which ought to be separated to a high degree (> 95%) before it reaches the actuators as it could negatively affect the actuators controllability.

The second problem is that aeration of the oil occurs to some extent after it is evacuated from the actuators. It is important to separate the air bubbles from the oil before it re-enters the actuators, as air, being compressible, impairs the performance of the hydraulic fluid when it acts to maintain the valves in an open state, as oscillations starts to occur (see figure 1.2). The oscillations are an unwanted phenomenon since they have a detrimental effect on the controllability of the valve curve.

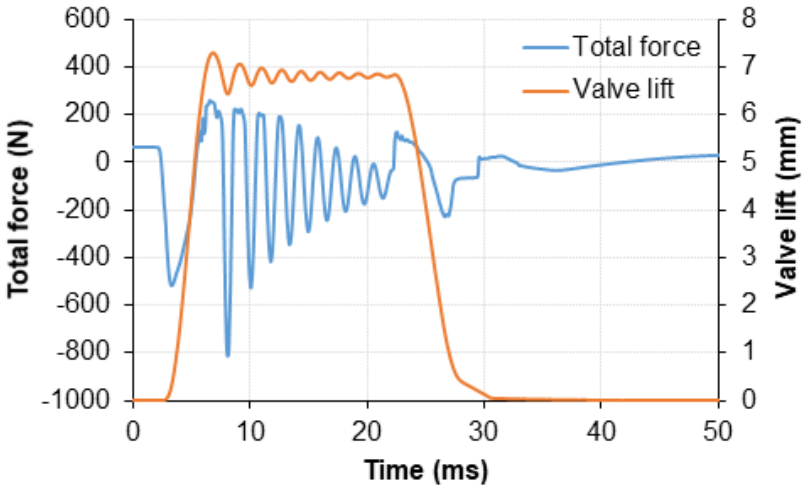

Figure 1.2: Simulations of the oscillations occurring during actuation.

1.3 Purpose

The purpose of this thesis work is to analyse and find suitable concepts to deal with the problem of deaeration and oil separation and to gain a good theoretical understanding of the problem. Good engineering practice will be applied in this situation by for example doing a thorough analysis of the problem, conducting a literature study of concurrent knowledge, evaluating different concepts in regard to system requirements, test said concepts to evaluate their actual performance and comparing the empirical results to the analyses.

1.4 Caveat regarding Non-disclosure agreement

Due to the current state of the system, as it is in the development phase, many parts of the system are subject to secrecy and a Non-disclosure agreement (NDA) has been signed in advance of the commencing of the project. Therefore, there are technical details that cannot be described in detail, especially regarding the design of the actuators, their performance, and the vehicles in which they are to be implemented.

2 Concept generation and Design

As an initial step in approaching the problem, overall system requirements were first formulated and quantified in order to get an understanding of the different parameters affecting the problem. Thereafter, several different concepts were analysed and evaluated for suitability for the specific problems at hand.

2.1 System requirements – Oil separator

The oil separation system must be able to conform with the following requirements set in cooperation and consultation with the company and intends to cover a wide operating range. This is due to the exact vehicle platform not being decided upon at the time of writing this report.

Table 2.1: System requirements for the oil separation system.

Parameter	From	To
Volumetric flow oil	0 litre/min	5 litre/min (relative density @20°C)
Volumetric air flow	10 litre/min	350 litre/min
Air flow Temperature	Ambient	120°C
Working pressure (gauge)	8 bar	20 bar
Allowable pressure drop	n/a	300 mbar
Inlet and outlet diameter	19 mm	

Additional non-quantifiable requirements were expressed as follows:

- The system must be passive, i.e. not have any power usage other than the inherent pressure drop associated with the volumetric air flow.
- It is required of the system to be easily packaged and lightweight. These parameters are however not quantified and will be under evaluation for the extent of the thesis work.
- Must be manufacturable in a viable way regarding mass production, for example casting, 3-axis CNC milling or turning.

- The requirement regarding the pressure drop is according to models and simplified simulations in CFD.

2.2 Concepts for oil separation

2.2.1 Impact separator

This concept uses a spring and pressure plate to limit the flow speeds through the separator. The reduced flow speeds make it possible so that oil droplets can collect and merge with each other through coalescence. The larger drops can then fall and exit through the bottom outlet. The addition of moving parts might have an impact on reliability and cost of the separator unit in a negative way.

Figure 2.1: Cross section view of impactor type crank house gas separator [2].

2.2.2 Filtration based solutions

Another possibility is to use a filter-based solution, either on its own or as a complement to another concept. Possible versions include using casted porous metal where the pore size can be determined for a certain maximum pressure loss, or a fine metal mesh. In the case of porous aluminium, it is possible to cast it in salt with a specified particle size in order to get a specified filter rating. Both concepts could be quite adaptable which means that there is much room for iteration.

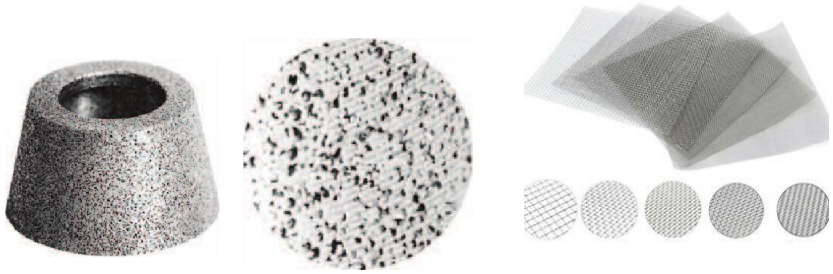

Figure 2.2: An example of a porous aluminium filter and steel mesh of varying grades.

2.2.3 Cyclone separator

The working principle of the cyclone separator is based on separating oil droplets utilising their inertia to separate it from the air. Using some simplifications, it is possible to calculate the required velocity to separate a droplet of a certain size from the airstream. There are versions with and without moving parts and can be sized to fit many different flow situations. Cyclones are generally used for larger sized droplets as well which fits with the requirements for this project.

2.2.4 Currently used separator setup

The separator currently used is a commercial design as shown in figure 2.4, also known as a Turboil separator. The separator works by allowing the air/oil mixture to enter from the top while passing through a spiral of fine metal brushes. This captures the small oil droplets and allows them to merge with other nearby droplets due to coalescence. The larger droplets can at this point fall into the lower chamber of the separator unit where it can exit through the lower outlet. The air curves sharply around the inside pipe section and exits through the upper outlet. The strong curvature of the streamlines also helps to separate any leftover oil in the air stream due to inertial effects.

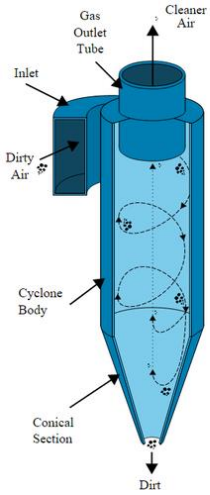

Figure 2.3: Schematic view of a cyclone separator [3]

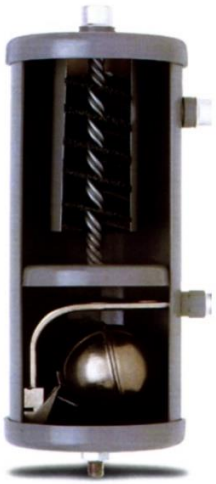

Figure 2.4: Cross-section of the “Turboil”[4]

2.3 Choice of oil separator concept

The chosen concept for oil separation from the air stream is a cyclone separator. This was chosen since it is a reliable concept which allows for small packaging. The other solutions were also generally more suited for smaller oil fractions, often in the form of mist and not, as in our case, in the form of a constant stream. However, other concepts working on the premises described above were said to be prepared for testing if time allows it.

A modular prototype will be used in order to test and see what parameters affect the separation efficiencies and pressure losses for different configurations. The prototype will feature three different cone sections and two different outlet tube sections which in total enables six different types of cyclones to be tested. The different inserts will be contained by a pressure tested vessel in order to safely run tests to upwards of 20 bar.

The aim of the study is to establish a relationship between geometric parameters in order to show where future improvements can be made to the design of the cyclone separator. A first design suggestion based on these findings is also to be presented. A more in-depth reasoning into the theory, design and analysis behind the cyclone separator is presented in chapter 3.

2.4 System requirements – Deaeration device

The deaeration system must be able to conform with the following requirements set in cooperation and consultation with the company and intends to cover a wide operating range. This is due to the exact vehicle platform not being decided upon at the time of writing this report.

Table 2.2: System requirements for the deaeration system.

Parameter	From	To
Volumetric flow oil	0 litres/min	0,5 litres/min
Working pressure (gauge)	4 bar	12 bar
Max temperature	100°C	
Allowable pressure drop	Should be negligible/close to zero	
Oil reservoir volume	At least 0,5 litres of oil	

Additional non-quantifiable requirements are as follows:

- The system must be passive, and not have any power usage other than the power used by the oil pump.
- It is required of the system to be easily packaged and lightweight. These parameters are however not quantified and will be under evaluation for the extent of the thesis work.
- The concept must, after additional development, be manufacturable in a viable way regarding mass production, for example casting, 3-axis CNC milling, turning, etc.

2.5 Concepts for deaeration

2.5.1 Hydro-/Vortex separator

A cyclone concept very similar to the concept already mentioned for oil separation may be used for deaeration purposes as well. Referred to either as a “Hydro cyclone” or as a “Vortex separator” in literature, it works in the same way as a cyclone separator. The air that is introduced into the flowing medium is collected in a low-pressure region in the centre of the converging part of the separator while the oil flows towards the outer sections due to the centrifugal force acting on it. The air can then be extracted through a vented port while the now deaerated oil continues to flow downstream from the separator.

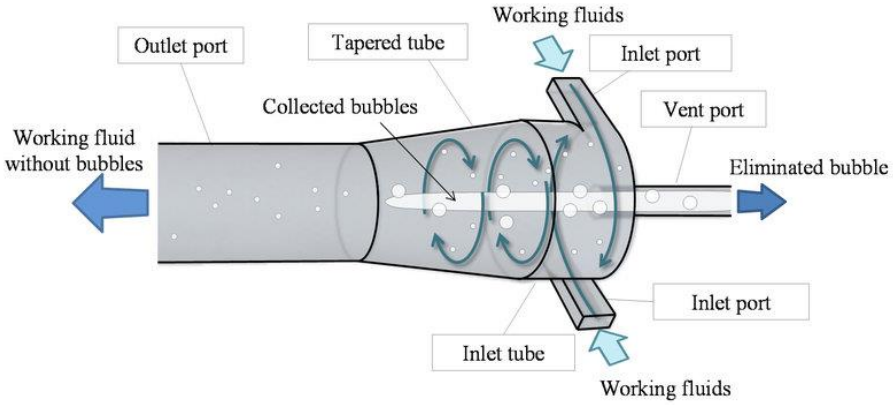

Figure 2.5: Working principle of a hydro cyclone/vortex separator [5].

2.5.2 Coalescence based solutions

Deaeration of the oil can be achieved with a filtration solution similar to the filtration concepts proposed for the oil separation case, where smaller bubbles through the process of coalescence can accumulate to form larger bubbles [6], which in turn are easier to separate. In order to ensure well suited coalescence conditions for the bubbles, some kind of filter or structure may be put in place in order to slow down the flow and/or catch bubbles passing through. Solutions such as porous aluminium and meshes may be utilised here as well.

2.6 Choice of concept – Deaeration system

The choice of deaeration system was made by going through the possible concepts and determining what could work in the desired application and examining the factors improving deaeration, which will be explained in detail under the heading 3.1.3. The concepts chosen for further testing are as follows: a cylindrical tank with an inner diameter of 100 mm, and a tube with an inner diameter of 38 mm in which several different inserts can be placed in order to evaluate each insert.

In short, the cylindrical tank is interesting to investigate as it can be shown that slowing the oil flow can greatly increase the amount of air which can be separated as the drag force acting upon a bubble is directly proportional to the velocity of the oil. Therefore, assuming that the velocity gradient across the diameter is somewhat stabilised, the drag force is inversely proportional to the square of the diameter of the tank.

For the smaller diameter cylinder, two different concepts were to be tested: one based upon leading the oil through a spiral and the other one where the oil passes over several mesh baffles. The idea behind the spiral was to increase the surface area which the oil is exposed to, which could lead to bubbles accumulating and coalescing at the surfaces. The principle working behind the baffle concept is also coalescence, where smaller bubbles could collect at the surface of the mesh baffles as the oil passes through and over them.

3 Theoretical study

3.1 Freevalve system functionality

The Freevalve system is operated by activating several solenoids in a specific order to eject the valve, maintaining the valve in an open state, and then by closing the valve. It is the pneumatic system that serves to open and close the valve, and the hydraulic system that keeps the valve in an open state. After each cycle, the air and oil are ejected from the actuators and the cycle repeats. The compressor currently used in the test rig is the TRSA12 by Sanden, a scroll-type compressor.

The oil used in the laboratory system is Mobil Rarus SHC 1026, an air compressor oil usually recommended for use in screw-type air compressors. This oil was chosen for several reasons, for example its viscosity characteristics and oxidation resistance which specify that it can operate up to temperatures of 200°C. Further temperature dependent characteristics can be found in Appendix 2.

It was early on established that the oil that needed to be separated from the airstream was mostly flowing along the edges of the tubes and not in the form of a mist. This was confirmed both by visual examination of the air stream through sight glasses placed at different points in the test rig.

3.2 Aerodynamics and fluid mechanics

The flow character has a big impact on possible assumptions and how to set up the problem which means that the Reynolds number must be specified according to equation 1. The radial velocity was estimated from CFD streamline results in order to get a rough approximation of the outwash speed experienced by the particles. Note that the Reynolds number is only used as a rough indication of the flow conditions. The density and viscosity values used are properties for the fluid medium flowing around the particle which is air in this case. Note that the dynamic viscosity is used in table 3.1 and that it is assumed to be independent from the

pressure acting on the medium. The particle diameter is in this simplified case assumed to be 10 μm which is considered coarse in aerosol terms.

$$R_e = \frac{\rho V D}{\mu} \qquad \text{(Eq. 1)}$$

Table 3.1: Parameters used to characterise the flow type and calculate the particle Reynolds number, for pressures.

	V_{radial} [m/s]	ρ [kg/m^3]	μ [Pa*s]	Re, particle
20 bars	3	18,64	22,64 *10-6	25

Table 3.2 shows a clearly turbulent flow inside the cyclone chamber due to the high Reynolds number. Instead of the particle diameter, both the inlet- and separator diameter is used to derive a resulting Reynolds number. This is a somewhat uncertain number but is consistent with the magnitude of Reynolds numbers approximated in cyclone separator applications in other studies [7].

Table 3.2: Parameters used to characterise the flow type and calculate the Reynolds number.

D [m]	V [m/s]	ρ [kg/m^3]	μ [Pa*s]	Re
19*10^{-3}	12	18,64	22,64*10^{-6}	218 000
80*10^{-3}	1,2	18,64	22,64*10^{-6}	79 000

3.2.1 Cyclone theory

A cyclone separator works by letting the air stream containing a second particulate or liquid phase enter the cyclone chamber tangentially to produce a swirling flow inside the chamber. The flow will then start to circulate to the bottom of the device and accelerate due to the converging section, thus increasing the rotational speed of the cyclone [8]. A separator properly designed for the operating conditions will force the other phase (particulate or liquid) out towards the outside walls before it finally can fall or flow to the outlet in the bottom of the chamber. The air stream, which should be free from the second phase given the right conditions, will reverse and exit through the top of the device due to the formation of a strong upwards central vortex.

As minimisation of pressure losses are desirable, and in order to get a reasonable estimation of the pressure losses, empirical models tested against experimental data were used. This allowed for early estimates of the pressure loss in order to compare CFD results with an insight into what parameters are important in designing the device with minimal pressure loss in mind. The notations shown in figure 3.1 will be used when referring to cyclone dimensions.

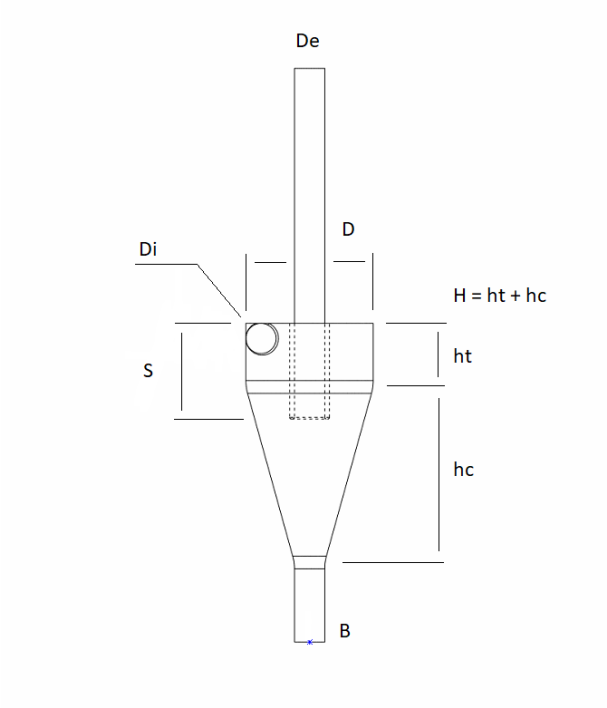

Figure 3.1: Cyclone dimension notations.

The Lapple equation is the first work done about modelling pressure losses in cyclones and is a very rough estimation with few parameters. Better models have been formulated over time and the one from (Dirgo, 1988) should provide a much better estimated pressure loss according to comparative studies [9].

Other common models such as the models by Stairmand and First found in comparative studies have been used to see what geometrical properties might affect the pressure loss the most [10]. The "H_v"-term is the cyclone head loss where the energy loss over the cyclone is equated to a static column of fluid.

$$\Delta P = \frac{1}{2}\rho_{air} {V_i}^2 H_v \quad \text{(Eq. 2)}$$

$$H_v = 16\frac{A_{inlet}}{{D_e}^2} \quad \text{(Eq. 3, Lapple)}$$

$$H_v = 20\frac{A_{inlet}}{{D_e}^2}\left(\frac{(S/D)}{(H/D)(h/D)(B/D)}\right)^{1/3} \quad \text{(Eq. 4, Dirgo)}$$

$$H_v = 12\frac{A_{inlet}}{Y{D_e}^2}\left(\frac{hb*hc}{D^2}\right)^{-1/3} \quad \text{(Eq. 5, First)}$$

$$H_v = 1 + 2\varphi^2\left(\frac{2(D-D_i)}{D_e} - 1\right) + 32\left(\frac{A_{inlet}}{\pi {D_e}^2}\right)^2 \quad \text{(Eq. 6, Stairmand)}$$

The Stairmand equation requires two additional equations presented below, φ and A where a friction factor, λ is estimated to 0,005 according to the paper.

$$\varphi = \frac{A_{inlet}}{2\lambda A}\left(\left(\frac{D_e}{2(D-b)} + \frac{4\lambda A}{A_{inlet}}\right)^{0,5} - \left(\frac{D_e}{2(D-b)}\right)^{0,5}\right) \quad \text{(eq. 7)}$$

$$A = \frac{\pi}{4}\left(D^2 - {D_e}^2\right) + \pi D h_b + \pi D_e S + \frac{\pi}{2}(D+B)\left({h_c}^2 + \frac{1}{4}(D-b)^2\right)^{0,5} \quad \text{(eq.8)}$$

Unless otherwise stated, the following dimensions and physical properties are used when presenting data from calculations. The cyclone outer diameter and height was set with what was desired from a packaging point of view with input from the engineers at Freevalve.

Table 3.3: Standard dimensions and physical properties used during calculations.

Cyclone diameter, D [mm]	**Cyclone total height, H [mm]**	**Inlet/outlet diameter, Di/De/B [mm]**	**Air dynamic viscosity [Pa*s]**	**Oil density at 120°C [kg/m3]**
80	150	19	22,64 *10-6	805,3

Previous work has been done on formulating a model for predicting separator efficiency and a particle "cut off" diameter. The large amount of oil for the application in this assignment makes this approach less viable but may still be useful for benchmarking concepts against each other.

The model presented below is commonly referred to as the Lapple "cut off" diameter [11]. The model is used for finding the particle size a specified cyclone can separate with 50% efficiency. The parameter "N" is an estimation of the amount of turns a given particle is subjected to inside the cyclone chamber.

$$N = \frac{1}{H}(h_t + \frac{h_c}{2}) \qquad \text{(Eq. 9)}$$

$$d_{p50} = \sqrt{\frac{9\mu D_i}{2\pi N V_{inlet}(\rho_{liquid} - \rho_{air})}} \qquad \text{(Eq. 10)}$$

It can be seen from the equations above that increasing the tangential velocity in the swirling flow as well as the amount of turns the stream is subjected to inside the chamber is the most effective way of improving the separator performance. There are other factors at play here but many other parameters such as viscosity, density and inlet dimensions are set due to current operating conditions and design decisions already made earlier in the design process.

Another simplified way of looking at the possible particle separation size is by looking at the problem from a static free body diagram perspective. In order to separate a given particle, the centrifugal force acting on it must be greater than the drag acting radially on the particle. This will make the particles collect at the outside of the cyclone and drain through the bottom outlet.

Since the Reynolds number with some margin for error is approximated to be between $8*10^4$ and $2*10^5$, a coefficient of drag of 0,47 is assumed in accordance with *Introduction to fluid mechanics* by Young, Munson, Okiiski and Huebsch [12]. It can be seen in figure 3.2 however, that there is a region at high Reynolds numbers where the "Drag crisis" phenomenon is present which might affect results drastically. "Drag crisis" refers to the region where drag coefficient drops off dramatically at high Reynolds numbers. The Reynolds number for the swirling flow is used in order to estimate the drag coefficient with this method. This method would be applicable on normal spherical objects but an alternative approach will be looked at due to the behaviour of small oil particles introducing more unknowns.

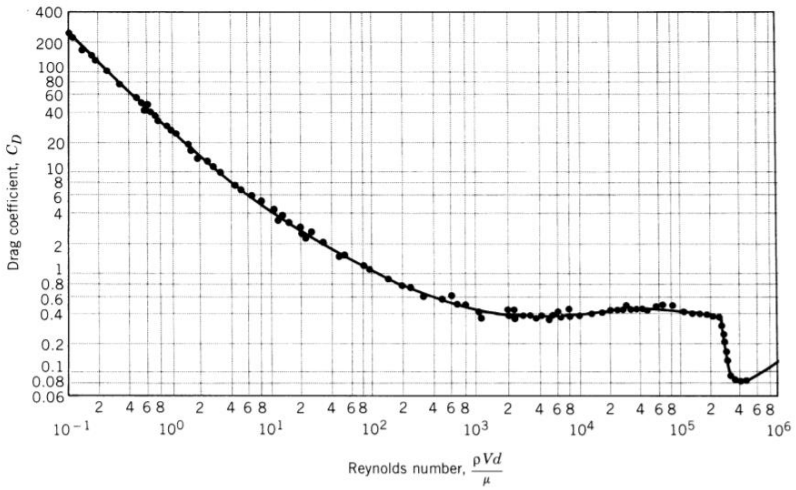

Figure 3.2: Drag coefficient of a spherical object as a function of the Reynolds number [12].

Stokes drag with a C_D value of 1 is often assumed regarding small particles with low (Re < 1) particle Reynolds numbers [13]. If other particle Reynolds numbers are estimated, expressions estimating the drag coefficient may be used which constitutes another approach in approximating the drag coefficient. With the particle Reynolds number at 20 bars previously shown, a C_D value of approximately 2,6 is given from eq. 11. In order to be on the more conservative side as a higher drag coefficient will lead to bigger cut off diameters according to equation 14, a C_D value of 2,6 is used from here on out.

$$C_D = \left(0{,}324 + \frac{21{,}9416}{Re_p{}^{0{,}718}}\right) Re_p/24 \qquad \text{(Eq. 11, Drag estimate, } 4 < Re_p < 2000\text{)}$$

$$F_c = \frac{m_p {V_T}^2}{R} \qquad \text{(Eq. 12, Centrifugal force)}$$

$$F_d = 6\pi C_D \mu V_R r \qquad \text{(Eq. 13 Drag acting on particle, Re > 1)}$$

$$d_{cut} = 2\sqrt{\frac{9\mu R C_D V_R}{2\rho_{particle} {V_T}^2}} \qquad \text{(Eq. 14, Particle cut off diameter, Re > 1)}$$

3.2.2 Deaeration mechanisms

Several factors must be considered when deciding where to position the deaeration device in the oil circuit in order to minimise the amount of air in the oil. Both in the form of free bubbles and as a solute. For example, the temperature and pressure of the oil must be taken into consideration as it varies strongly depending on where in the circuit the oil is. According to Henry's law [14], the solubility of gases decreases with decreased pressure and increased temperature, which speaks for performing the deaeration just after the oil has evacuated the actuators as it is here that the oil is at its minimum pressure and maximum temperature.

Another mechanism benefiting from higher temperatures is the reduction of drag force acting upon bubbles in the direction of the oil flow, as higher temperature drastically decreases the viscosity of the oil and thereby reduces the drag which acts to pull the bubbles along the flow (see equation 18 and appendix 2). Finally, the buoyant force acting on each bubble in opposite direction of the flow is significantly increased for a larger diameter of the bubble. Deaeration is thereby benefited by a lower pressure and higher temperature as the air expands more compared to the oil (see equation 17). Assuming laminar flow over a single bubble and that no other vertical acceleration is taking place, only these two forces will be acting on the bubble in the vertical direction.

In order to further quantify how the parameters (temperature, pressure, oil flow, etc.) affects the possible concepts, a free body diagram of a single bubble with related force equations were set up (see figure 3.3). The bubble can be assumed to be completely spherical due to the very low Galilei and Eötvös numbers, as can be seen in equations 15 and 16 as well as in figure 3.4 [15]. Due to this fact, the drag coefficient can be calculated as that of a sphere.

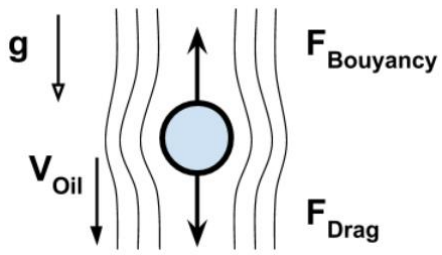

Figure 3.3: Forces acting upon a single bubble.

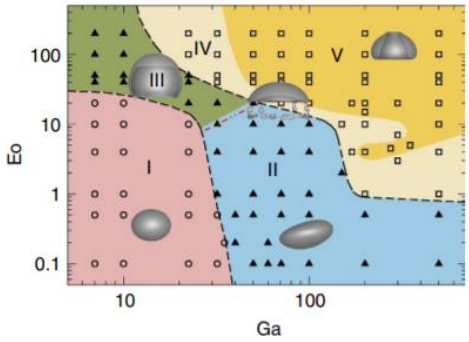

Figure 3.4: Bubble shape regions. [15]

The maximum value of the Galilei- and Eötvös numbers are calculated, with data from the tank diameter sweep (see figure 3.8) as it yielded the largest bubble diameters. The only unknown variable is the surface tension value, which is assumed to be no less than $15*10^{-3}$ N/m [16].

$$Ga_{max} = \rho_{oil}\sqrt{g\frac{d_{bubble}}{2}} * \frac{d_{bubble}}{2\mu_{oil}} = 9.8 * 10^{-5} \quad \text{(Eq. 15)}$$

$$Eo_{max} = \rho_{oil} g \frac{{d_{bubble}}^2}{4\sigma} = 6.6 * 10^{-4} \quad \text{(Eq. 16)}$$

The forces acting in the vertical direction on a bubble suspended in oil in a cylindrical container with a flow going from top to bottom, assuming that the vehicle is not experiencing any vertical accelerations, is the buoyant force due to the lower density and the drag force acting on the bubble due to the oil flowing past the bubble. Logically, a larger bubble will easily travel upwards despite the drag as this can easily be seen by examining equations 17 through 19. The buoyant force is proportional to the cube of the diameter of the bubble, whereas the drag force is directly proportional to the diameter of the bubble [13].

$$F_{buoyant} = \frac{\pi}{6}{d_{bubble}}^3(\rho_{oil} - \rho_{air})g \quad \text{(Eq. 17)}$$

$$F_{drag} = 3C_D\pi\mu_{oil}d_{bubble}V_{oil} \quad \text{(Eq. 18)}$$

$$d_{cut} = \sqrt{\frac{18\nu V_{oil}C_D\rho_{oil}}{(\rho_{oil}-\rho_{air})g}} \quad \text{(Eq. 19)}$$

A cut-off diameter can therefore be calculated for a given cylindrical container at specific conditions, defined as the diameter of a bubble which experiences net-zero forces in the vertical direction. Any bubbles larger than this diameter should therefore eventually rise to the surface. It should be noted that these calculations are somewhat simplified, as they disregard no-slip conditions near walls and assumes a stabilised flow over the cross section of the cylinder. However, several factors can be swept to gain a better understanding of the factors affecting the cut off volumes of bubbles, see figures 3.5 through 3.9.

The values that are stationary during a parameter sweep are as follows: The working pressure is 6 bar, the temperature is 120°C, the volumetric oil flow is 0.5 l/min and the tank diameter is 7 cm. Bubble sizes are normalized to 300 bar and 120°C, as these are the conditions which will be experienced in the actuators.

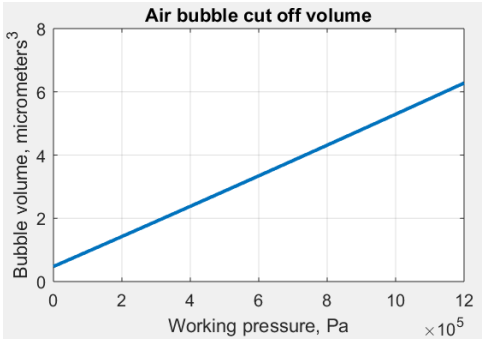

Figure 3.5: Effect of pressure on deaeration.

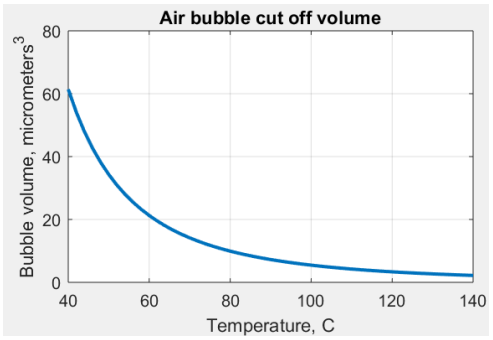

Figure 3.6: Effect of temperature on deaeration.

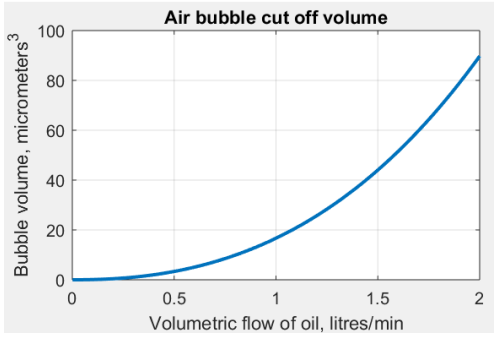

Figure 3.7: Effect of oil flow on deaeration.

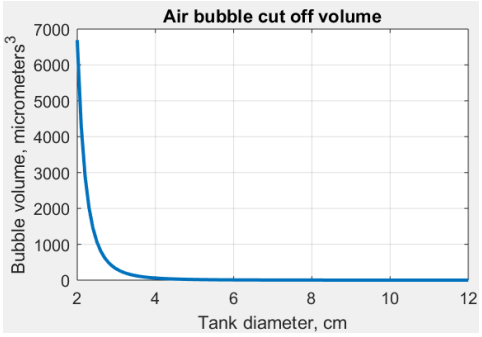

Figure 3.8: Effect of tank diameter on deaeration.

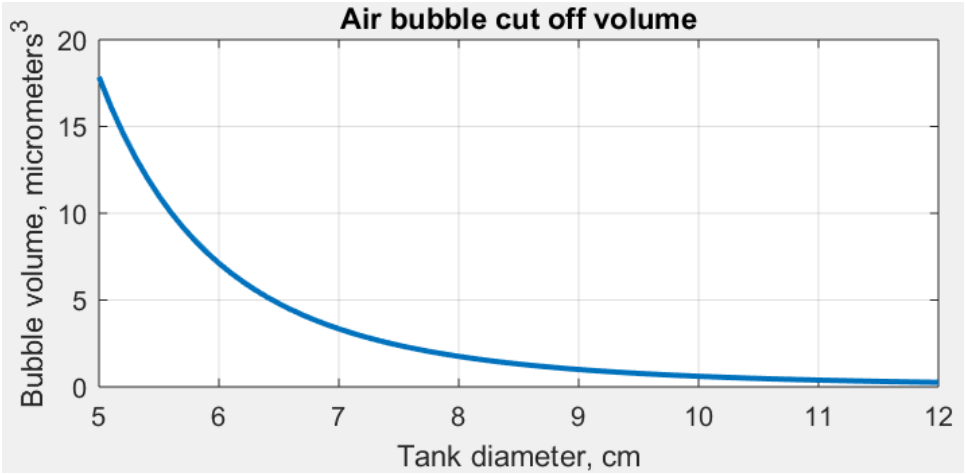

Figure 3.9: Close up of tank diameter effect of deaeration.

4 Simulations and testing

4.1 Numerical simulations

An experiment-based approach was mainly used during this project in order to validate the separator performance, with focus on design iteration. These design iterations were created with CAD and evaluated by using computational tools such as CFD to better understand the flow inside the device and in order to quantify certain parameters such as pressure drop over the device and maximum tangential velocity for cyclone-type separators. The ambition was to correlate certain parameters such as rotational velocity or pressure distribution with how the concepts performed in real life testing. The iteration process could be speed up significantly if such a trend could be identified. Since this requires the use of much computational power, the Lunarc computational cluster was used to speed up the process.

Two-phase and transient simulations were looked at early on during the project but was ultimately discarded as the workload was deemed far too heavy with little payoff compared to practical testing of prototypes which were to take place regardless of the possible results of such a simulation. Design suggestions in CFD are evaluated based on flow speeds achievable in the rotating air stream, pressure distribution inside the separator chamber and the estimated pressure loss over the entire device.

4.2 Setup and Boundary conditions

The goal for this thesis project was not to develop and validate a CFD model. The aim was to create with a model accurate enough to see rough parameter trends in relation to certain parameters such as pressure loss over the device and flow speed inside the separation chamber. Inlets and outlets were set to 19 mm as those interfaces were already set by the company. This allowed for the inlet boundary condition to be specified as a velocity flow also seen in table 4.1. Parameters of the mediums are based on the operating conditions specified below.

Table 4.1: CFD setup conditions.

Parameters	Values
Temperature [°C]	120
Pressure [bar]	20
Inlet velocity [m/s]	12
Outlet [bar]	0 (gauge pressure)

Relaxation factors are applied to the different equations the CFD code is trying to solve when the residuals start to become unsteady. The hope is that by applying these factors on the residuals before the next iteration, a more stable solution can be found. This is however highly situational and mesh dependent which means that there is no easy way to predict what a "good" relaxation factor would be. In the simulations run for this thesis project, it was found that a lower under relaxation factor of 0.3 compared to the default of 0.7 helped with the residual convergence which otherwise developed oscillating behaviour over time.

In order to capture certain turbulent flow characteristics, a turbulent length scale value could be specified. This should be large enough to capture the eddies present in any turbulent flow and was set to 0,75 mm using existing rules of thumb [17].

Early simulations had problems with reversed flow at the outlet of the geometry which is something that lead to early convergence issues. The strategy to combat this behaviour was to place a volumetric control on the mesh closest to the outlet. By elongating and making the cells larger in this region, reversed flow was mostly eliminated and the negative effect it had on the convergence of the solution was greatly reduced.

Since the real operating conditions at the outlet of the device is unknown and since some sort of boundary condition must be placed at the outlet, compromises had to be made. The outlet was modelled as a pressure outlet with a gauge pressure set to zero with the inlet being defined as a velocity inlet. Ideally, it would have been optimal to not prescribe any value to the pressure at the outlet. Instead, the outlet section was extended significantly, and the pressure loss was subsequently measured at different points to compare the results. This also helps with the phenomena of reversed flow at the outlet.

Increasing the gas (air) density to what would be present at 20 bars and 120°C affected the convergence time in a very negative way. However, studies done on cyclones in elevated pressures exhibit a linear increase of pressure drop with an increase in pressure inside the chamber [18].

In order to get rough estimates of pressure drop from CFD, the analysis is run at conditions representative of 120°C and atmospheric pressure with a factor added on to compensate for the pressure condition.

The y+ value of a cell/mesh determines how the near wall behaviour of the flow needs to be modelled. If possible, it is desired to keep the y+ value below 5 in order to model observed experimental behaviour in the boundary layer. This will keep flow behaviour in the linear "viscous sublayer" region, meaning that no wall functions are needed to model the boundary layer.

4.2.1 Turbulence models

The available turbulence models of interest in Star-CCM+ are K-omega, K-epsilon and Reynolds-Averaged Navier-Stokes. The type of flows that will be examined in most, if not all, of the simulations will be characterised by strong curvature and a heavy swirling flow. Other models such as LES (Large eddy simulation) are discarded directly since they are computationally expensive and out of the scope of this thesis. A brief overview of the models will be presented here with a more in-depth mathematical derivation being outside the scope of this thesis work.

Both the K-omega and K-epsilon turbulence models are so called two equation turbulence models, meaning that they solve two transport equations in order to simulate the flow characteristics in a turbulent flow. The variables for these two equations are the turbulent kinetic energy and turbulent kinetic energy dissipation.

The K-epsilon "realisable" model also solves the two transport equations described above with the kinetic energy formulation being the same as for the standard case. However, the formulation for the turbulence energy dissipation is different and the turbulent viscosity is modelled with an equation rather than being an empirically set constant as with the standard formulation of the turbulence model.

The final model evaluated was the Reynolds stress model which solves the two transport equations with an additional 6 Reynolds stress components to account for momentum fluctuations due to turbulent flow. This turbulence model should yield more accurate results but is much more computationally expensive due to the added equations that must be solved for each iteration. Achieving convergence is also harder compared to the simpler models described above.

In the end, the K-epsilon realisable turbulence model was chosen due to sufficient performance and easier convergence than the other models tested.

The literature study suggested that the swirling flow inside a cyclone separator is of a transient character but has little effect on the result and accuracy of the CFD solution [19]. This is tolerable with the set scope for this project and thus, transient effects will not be looked at in CFD for this thesis work.

4.2.2 Mesh study

After a suitable turbulence model and overall physics settings had been chosen, a mesh study was performed in order to find a model which allowed repeatability when comparing different designs. This also meant that computation time could be saved by not running an unnecessarily fine mesh in order to get reasonable results.

Both a trimmer and polyhedral meshing strategy was investigated. The polyhedral mesher seemed to create a better converging solution overall and was less sensitive to changes in the separator design and various physics parameters. The polyhedral mesher is also referred to in the Star CCM+ documentation as suitable for "internal swirling flow". The parameters of interest were chosen to be pressure drop and flow speed in the top part of the separator with the result shown in figure 4.2. The simulations had to be run for 15000-20000 iterations in order to be considered as converged with some variation due to the mesh size.

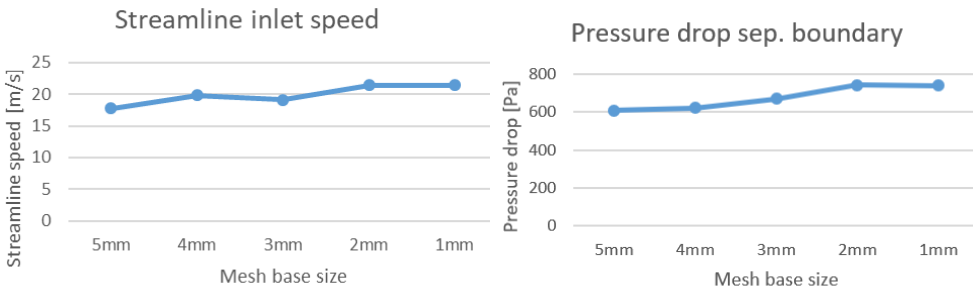

Figure 4.2: Mesh convergence study of cyclone separator.

4.3 Physical testing methods

Physical testing was conducted in order to evaluate the designs. The rig, as described below, was first rigorously tested in order to gain empirical knowledge and understanding of its functionality and behaviour before doing the modifications necessary to run the desired tests.

4.3.1 Oil separator test method

The compressor test rig, normally used to test the functionality of different models of scroll compressors, was used to test the oil separation capabilities of different devices. This rig, as schematically drawn below in figure 4.3, is built to represent the air circuit of the finalised product as closely as possible. This setup was chosen due to early testing showing that the Turboil separator had a separation efficiency of > 90% at relevant operating points.

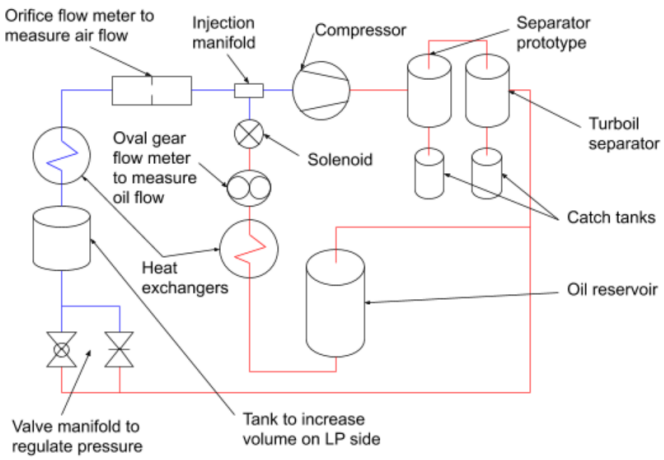

Figure 4.3: Setup for separation tests, red- and blue lines shows high- and low pressures respectively.

Optical readings and measurements of particle density or size were disregarded in this thesis work due to the high amount of oil in the air stream. The flow entering the separator was primarily a continuous flow along the edges which would have heavily disrupted such methods. The oil was therefore caught, as shown in figure 4.3, in separate catch cans during a test cycle and thereafter manually weighed. It is controlled during the test through a sight glass in the air stream, that the two separators in series will collect oil to such a degree that the amount of oil passing the separators is negligible.

Different operating points, as shown in table 4.2, were selected based upon the requirements of the separator and upon the conditions that could be reached with the limitations of the rig. The tests done for this thesis were conducted under 10 bar on the high-pressure side due to pressure limitations on certain installed components such as the tanks used to collect the oil. It is however very likely that a higher oil injection flow can be achieved with the system operating at the goal of 20 bar.

Table 4.2: Desired and achievable operating points for the oil separator.

Parameter	Lower value	Upper value (achievable in test rig)
Volume flow oil	0 litre/min	2 litre/min
Volume flow air	100 litre/min	388 litre/min

During a test cycle, several parameters were measured and logged in order to ensure that the desired operating conditions were met and to ensure that no anomalies were present. A "corrected" flow is presented in the results since the flow sensor used is normalised for an absolute pressure of 6,013 bar at a temperature of 80°C. This means that the output flow needs to be compensated regarding temperature and pressure estimated over the separator unit which will be different due to the flow sensor being placed further downstream in the system. The flow sensor used was an M3-series from Eletta.

4.3.2 Oil separator prototypes

A modular system was used for the prototype, as it was desired to test several different configurations and make data-based decisions. The design could be varied in three different ways, either by changing the bottom insert, by changing the top insert or by flipping the prototype upside down which effectively results in the inlet being positioned at a lower point. Due to time limitations, all possible permutations of inserts were not tested for all operating points. Instead, a Darwinian approach was taken during testing, so that the concepts with a lower degree of separation can be disregarded in an early stage in order for the better concepts to be subjected to more challenging operation points.

The outer shell was manufactured according to standards regarding high pressure containers (PN40 according to EN 1092-1) and pressure tested by the manufacturer before being used at Freevalve (see Appendix 1 for drawings).

The different designs that were to be evaluated via different inserts are schematically displayed in figure 4.4 where different combinations of these inserts were tested.

The steel mesh cylinder was constructed with a fine stainless-steel mesh graded to 0,18 mm. The notation used for different insert configurations are (Bottom insert/ Top insert/Inlet Low or High) in the results presented under heading 5.3. “C” is used to denote a cone while “VF” is used to denote a vortex finder, and “H” and “L” is used to denote a high and low inlet respectively.

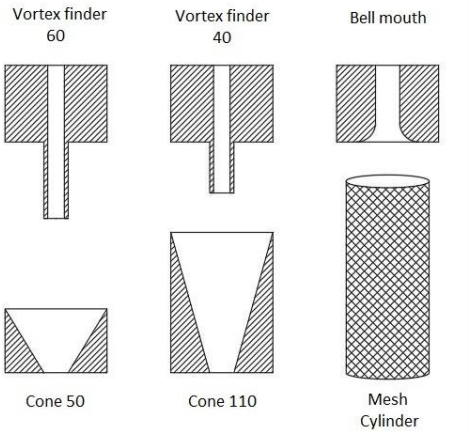

Figure 4.4: Schematic representation of concept inserts

4.3.3 Test cycle, oil separator

In order to ensure replicability, the test cycle for the separator tests was determined beforehand. The rig was first warmed up by running the rig with appropriate settings until the temperatures reached steady state. Due to the large variances in operating points, the temperatures for the system in steady state was found to be between 80 - 130°C. The methodology was the following:

1. Pressurise the system to specified pressure from the wall supply.
2. Start logging data.
3. Start the motor and set desired speed.
4. Adjust the valve to achieve the desired pressure ratio.
5. Start the oil injection with a predetermined duty cycle - start time keeping.
6. Let approximately 1 litre oil drain from injector supply - turn off oil injection and motor.
7. Stop logging data, depressurise the system.
8. Empty all catch cans in the system, measure collected oil mass with a scale.

4.3.4 Deaeration test method

The deaeration devices were tested in the compressor rig, as schematically drawn in figure 4.5. The deaeration of the oil was here evaluated by visually examining the oil in the circuit by letting the oil pass through a sight tube before and after the prototype.

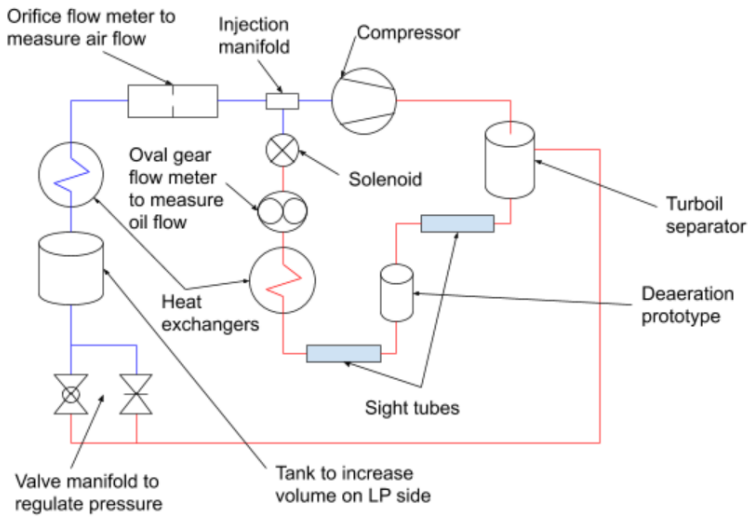

Figure 4.5: Setup for deaeration tests, red- and blue lines indicting high- and low pressure respectively.

In order to evaluate the efficiency of the deaeration device two sight tubes were mounted in the oil circuit, one just before and one just after the deaeration device. Through visual observation and photographic documentation, some conclusions could be drawn regarding the efficiency of the deaeration device.

The main factors affecting the deaeration of the bubbles is, as could be seen under the heading 3.1.3., the velocity and temperature of the oil, as well as the pressure surrounding it. As part of the purpose of the oil is to cool the system before the air stream returns to the compressor again, it is the intention that the oil will maintain a temperature of roughly 100°C in the oil reservoir. The rig will therefore be run until a steady state is reached and the oil observed in the sight glass is known to have passed through the compressor and deaeration device.

4.3.5 Deaeration prototypes

A tube with an inner diameter of 38 mm was used in which different inserts could be placed. Two helical inserts with two different pitch heights and a steel mesh baffle insert were tested and evaluated, see figure 4.6. The central channel is there to allow air to escape as it reaches the settling chamber at the bottom of the separator.

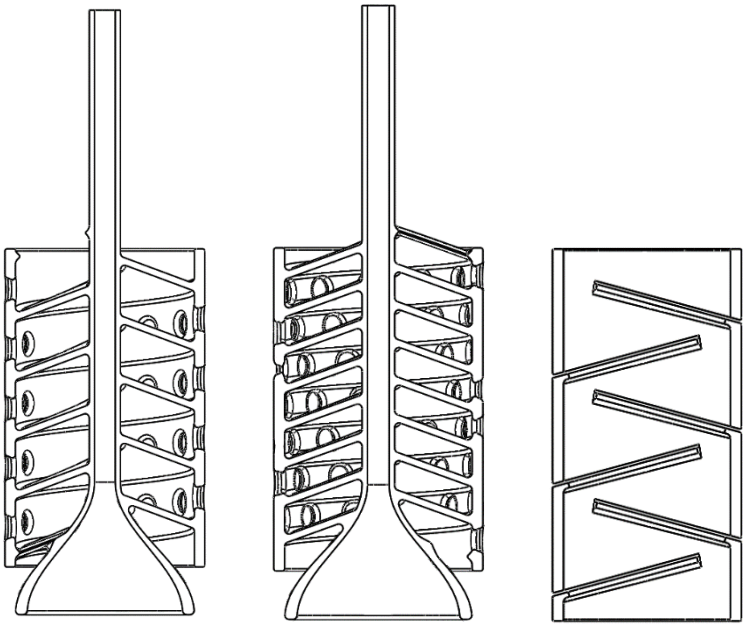

Figure 4.6: Cross-sectional view of inserts to be tested.

4.3.6 Test cycle, deaeration

1. Pressurise the system to 6 bars from the wall supply.
2. Start the motor and set desired speed, oil flow at maximum 0,5 l/min.
3. Let the system reach steady state.
4. Turn on backlighting behind sight glass.
5. Observe sight glasses in order to note possible differences in aeration.
6. Turn off the electrical motor driving the compressor.
7. Let the system depressurise.

5 Results

5.1 CFD results

CFD results showed no significant pressure drop difference between the different cyclone concepts which is consistent with what the pressure drop models predicted as well. The pressure drop at 20 bar working pressure is predicted to be between 0,1-0,2 bars for all configurations and is not deemed to be significant compared to other parts of the system.

Figure 5.1 shows the 110C/40VF/H cyclone concept which had the highest streamline velocity combined with the highest pressure at the cyclone walls. The pressure at the outside wall could be increased at the cost of a larger pressure drop but with a longer vortex finder. This did not contribute to a higher streamline velocity however which makes performance gains with this change unlikely. Note that the results in table 5.1 are at atmospheric pressure and thus needs to be multiplied by the pressure for accurate pressure loss results.

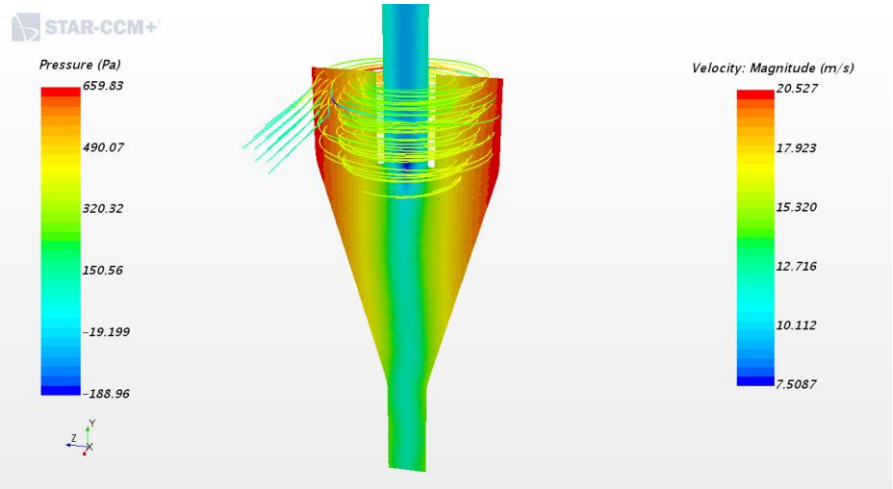

Figure 5.1: Cyclone 110C/40VF/H CFD result showing pressure distribution and rotational velocity.

Table 5.1: CFD results at atmospheric pressure.

Concept	Streamline velocity [m/s]	Pressure drop [Pa]	Pressure drop at 20 bars [bar]
110C/40VF/H	20,527	660	0,132
110C/60VF/H	20,243	695	0,139
50C/40VF/H	18,329	468	0,0936
50C/60VF/H	16,963	475	0,095

5.2 Analytical results

The following pressure drop results were obtained with the presented models for the cyclone separator, see table 5.2. The other non-cyclone concepts also tested are not believed to deviate significantly from this due to the set outer dimensions and overall similarities in geometry.

Table 5.2: Pressure drop [Pa] results at 20 bar working pressure for 110C/40VF/H cyclone concept.

Model	Lapple	Dirgo	First	Stairmand	Demir
P. loss [bar]	0.169	0.233	0.137	0.164	0.147

In table 5.3, velocity and parameters affecting the effective number of turns is changed in order to show how it affects the cyclone "cut off" diameter for the Lapple timed flight approach. The cyclone 50C/40VF/H concept was shown to be the best in this regard although there was little difference between all the cyclone concepts.

Table 5.3: Particle cut off diameter for different for specified dimensions and velocity conditions.

Height of cyclone top section	ht [mm]	40	40	100
Height of cyclone conical section	hc [mm]	110	110	50
Number of resulting turns in cyclone	N	0,63	0,63	0,83
Inlet velocity (based on 19 mm diameter)	[m/s]	12	8	12
Resulting particle cut off diameter	[μm]	10,14	12,42	8,84

Table 5.4 shows the effect increased tangential flow speed has on the particle cut off diameter based on the free body diagram method for the same 50C/40VF/H cyclone concept described above. The results seem reasonable compared with the cut off diameter for 50% separation efficiency in table 5.3 indicating that there is some merit to this approach as well. A radial speed of 3 m/s is assumed from CFD results, and the tangential speed is swept for three values.

Table 5.4: Particle cut off diameter for different streamline speeds for cyclone 50C/40VF/H.

Streamline speed in cyclone	[m/s]	15	20	25
Resulting particle cut off diameter	[μm]	37,5	28,1	22,5

5.3 Oil separator test results

The results for the first batch of separator concepts are presented below where each table consists of data taken at the same operating conditions regarding pressure, pressure ratio and oil injection. The compressor speed is then swept at three different points for each table where the testing is subsequently narrowed down to fewer but the more promising concepts. The notation used for the concepts are as mentioned earlier (lower insert / top insert / inlet position) when describing the different insert configurations. The cyclone configurations in bold below were run with the inlet at the top of the separator unit. The other test runs were instead run with the separator unit flipped around and the inlet at the lower part of the unit. The colour gradients of the tables are matched as to indicate the lowest degree of separation (red) as well as the highest degree of separation (green) of each respective table. The Cyclone concepts (in bold) did not show any significant difference in performance which meant that no correlation between Numerical results and efficiency could be found.

Table 5.5: Separator efficiency in % for 3,2 bars starting pressure / 3 pressure ratio / 0,6-0,7 l/min oil injection.

Compressor rpm	**110C/40VF/H**	**50C/40VF/H**	**50C/60VF/H**	Bell/50C/L
5500	95,4	96,6	97,4	98,4
7000	89,6	91	89,5	99,25
9000	85,6	85,9	88,4	98,6

Table 5.6: Separator efficiency in % for 3,2 bars starting pressure / 3 pressure ratio / 1,15-1,25 l/min oil injection.

Compressor rpm	**110C/ 40VF/ H**	110C/ 50C/H	50C/ 110C/L	Bell/ 50C/L	50C/ Bell/L	Empty/ Empty/ L	Empty/ VF40/L	Mesh cyl. /L	Empty /Mesh cone/L
5500	98	97,7	96,4	99,2	98,9	98	98,2	97,4	96
7000	94,4	92,7	74	98,1	94,3	99,4	88,8	86,9	90
9000	87,3	89	72,5	89,6	86,6	89,4	76,5	82,5	62,8

After the first test run, more detailed sweeps were performed on the Bell/50C/L concept as well as the 110C/40VF/H cyclone. Further dependencies between separator efficiency and other parameters involved were established with more detailed results presented below.

The efficiency is from here on plotted against the true flow rate over the separator for a more direct comparison of concepts. It is noted that once the air flow goes beyond 300 litres per minute, corresponding to an estimated 1 m/s vertical velocity inside the separator chamber, separator efficiency drops off dramatically. Likewise, flow rates under 200 litres per minute or about 0,6 m/s vertical velocity shows a similar drop off in efficiency. Table 5.7 through 5.9 contains the detailed results for the Bell/50C/L concept. Table 5.10 and 5.11 contains the same results for the 110C/40VF/H cyclone concept.

Table 5.7: Results for 3,2 bars start pressure and pressure ratio 3, Bell/50C/L concept.

Compressor rpm	**Air flow [l/min]**	**Corrected air flow [l/min]**	**Inlet speed [m/s]**	**Separator vert. velocity [m/s]**	**Separator eff. [%]**
7000	192	303,183	17,823	1,005	98,1
8000	220	347,398	20,422	1,152	93,3
8250	219	345,818	20,329	1,147	94
8500	219	345,818	20,329	1,147	90,5
8500	230	363,188	21,350	1,204	86
8750	246	388,454	22,835	1,288	74,4
9000	228	360,030	21,164	1,194	76,5

Table 5.8: Results for 4,2 bars start pressure and pressure ratio 3, Bell/50C/L concept.

Compressor rpm	Air flow [l/min]	Corrected air flow [l/min]	Inlet speed [m/s]	Separator vert. velocity [m/s]	Separator eff. [%]
3000	95	117,401	6,901	0,389	79,5
4000	122	154,806	9,100	0,513	84,5
5000	176	198,513	11,670	0,658	96,9
6000	205	240,777	14,154	0,798	98,6
8000	295	332,735	19,560	1,103	93,4
8500	299	337,246	19,825	1,118	87,5
9000	310	349,653	20,554	1,159	72,7

Table 5.9: Results for 5,2 bars start pressure and pressure ratio 3, Bell/50C/L concept.

Compressor rpm	Air flow [l/min]	Corrected air flow [l/min]	Inlet speed [m/s]	Separator vert. velocity [m/s]	Separator eff. [%]
4000	158	155,934	9,167	0,517	61,4
5000	197	199,979	11,756	0,663	87,3
6000	265	247,770	14,565	0,822	85,3
7000	270	261,032	15,345	0,866	86,5
8000	320	309,371	18,186	1,026	83,4
9000	390	364,643	21,435	1,209	62

Table 5.10: Results for 3,2 bars start pressure and pressure ratio 3, 110C/40VF/H cyclone concept.

Compressor rpm	Air flow [l/min]	Corrected air flow [l/min]	Inlet speed [m/s]	Separator vert. velocity [m/s]	Separator eff. [%]
3000	74	119,508	7,025	0,396	73,6
4000	96	151,592	8,911	0,503	84,5
5500	141	222,650	13,088	0,738	98
7000	180	284,234	16,709	0,942	94,4
9000	190	300,025	17,637	0,995	87,3

Table 5.11: Results for 4,2 bars start pressure and pressure ratio 3, 110C/40VF/H cyclone concept.

Compressor rpm	Air flow [l/min]	Corrected air flow [l/min]	Inlet speed [m/s]	Separator vert. velocity [m/s]	Separator eff. [%]
3000	100	114,611	6,737	0,380	54,3
5000	172	200,362	11,778	0,664	75,9
7000	242	286,603	16,848	0,950	88,4
8000	265	319,161	18,762	1,058	86,7
9000	325	355,293	20,886	1,178	84,7

Separator efficiency plotted against the corrected flow value displays a trend where both concepts loose performance at both too low and too high flow rates, see figures 5.2 and 5.3.

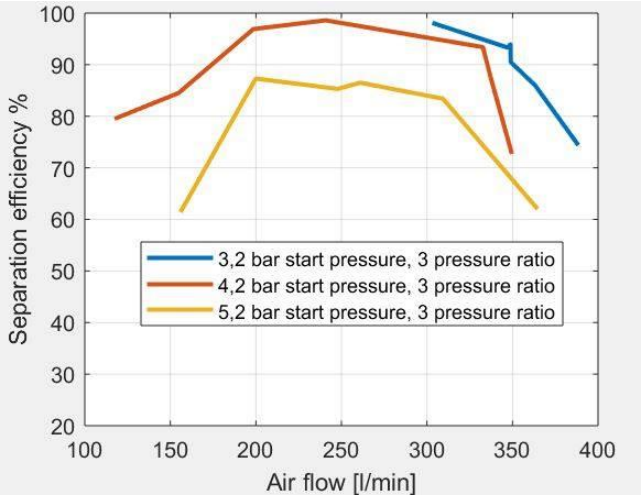

Figure 5.2: The Bell/50C/L separator concept efficiency plotted against flow rate for different pressures, corresponding to the data from table 5.7 through 5.9.

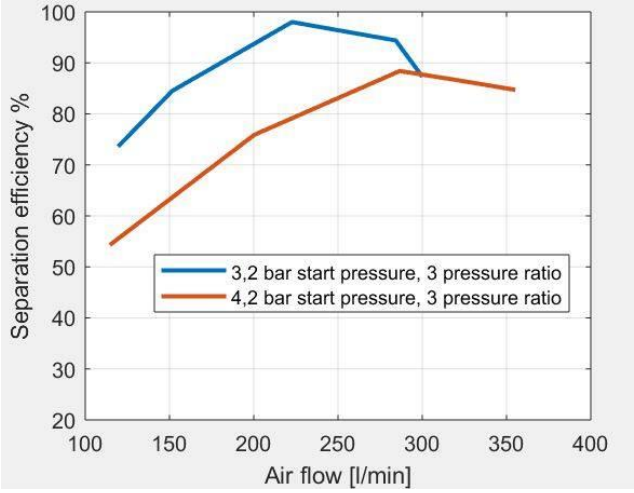

Figure 5.3: The 110C/40VF/H cyclone concept efficiency plotted against flow rate at different pressures, corresponding to the data from table 5.10 and 5.11.

5.4 Deaerator test results

The inserts were the first tested and through visual examination of the oil stream, it was deemed that the results were inconclusive with little to no decrease of air bubble quantity and volume identified through the sight glass. As can be seen in figure 5.4, there was a variation of bubble sizes which were estimated to be in the area of around 0.05 - 0.5 mm in diameter.

Letting the oil run through a larger settling chamber was also tested. As the system reached steady state, there was deemed to be a slight decrease of aeration of the oil stream. Due to the volume of the oil tank, it took several minutes before all the oil had circulated in the circuit.

It should be noted that there was air trapped in the sight tube during the start of all tests, which can explain some of the bubbles in the upper parts of the sight tube. However, all the tests were deemed inconclusive as to the effectiveness of the deaeration concepts due to the lack of data.

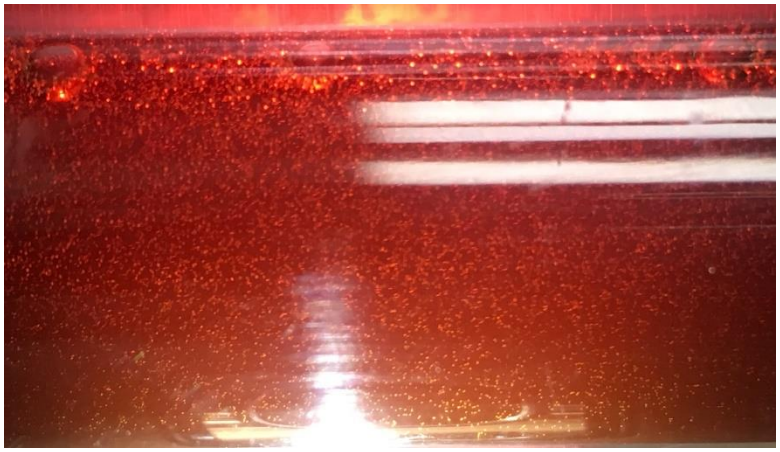

Figure 5.4: Air bubble sizes and quantities during normal running conditions in the test rig.

6 Discussion

6.1 Separator

As could be seen from tables 5.7 through 5.11, as well as in figures 5.2 and 5.3, a drop off in performance could be seen at both low and high flow rates of air, with a region in between where performance was better. This held true for both the Bell/50C/L- and 110C/40VF/H concepts which were more thoroughly tested. The data also indicates a drop off in performance at higher pressures although further testing is required to confirm or deny this. The air flow rate region of 200 - 300 litres per minute through the separator was shown to result in improved separation efficiency corresponding to an average vertical velocity of approximately 0,6 to 1 m/s in the separator chamber. This is the vertical velocities in which the concepts are recommended to be optimised for if it is decided to proceed with this development path. Pressure drop was deemed inherently quite low across all concepts and should thus not be a deciding factor for any major design decisions. The use of bell mouth profiles at inlets and outlets could still be applied for lower pressure drop at no separator efficiency disadvantage. The efficiency results for the separator concepts were too closely matched in order to accurately make any significant predictions with the CFD model as it is currently set up.

6.2 Deaerator

As equipment and time constraints led to using the compressor test rig instead of an actuator rig, testing and verification of the concepts were greatly compromised. Therefore, no conclusions can be drawn to whether the deaerators worked in any significant way or not. This is further discussed in the next subchapter, Possible improvements.

6.3 Possible improvements

6.3.1 Oil separator

It became apparent early on that the accuracy of the measurements, regarding the efficiency of the oil separators, depended greatly on how several unknown factors could be controlled for. Firstly, it was difficult to ensure that the return air was free from oil. Initially, several oil traps were installed in order to minimise the amount of oil circulating in the system, as any oil staying in the circuit was more likely to end up in the separator and therefore overestimating the efficiency of the separator. The final setup with the separator concept and the existing Turboil separator in series was visually determined with sight glasses to be sufficient.

Secondly, there were difficulties in maintaining a constant temperature for the return air and injected oil. The water supply for the cooling of the rig was installed in parallel with the water supply to all the other test rigs in the lab, which resulted in a varying degree of cooling. The cooling for the oil- and air circuit respectively on the compressor rig was also installed in parallel, and the balance of water flow between these heat exchangers was controlled only by a ball valve. Due to the temperature variations, the pressure also experienced some variations as an effect but was checked as carefully as possible before each test.

Furthermore, there were some other steady state issues occurring during early testing. Since the oil was mostly within its closed loop, it was slowly becoming more and more aerated. As the compressor rig is not featuring any actuators the bubbles themselves were only an issue when it comes to measuring the volume of the injected oil with an oval gear-type flow meter, whereby the bubbles increased the apparent volume of the oil over time. This problem, confirmed by visual confirmation of the oil stream through a sight glass, was first encountered in an earlier test setup where the oil returning from the separator was routed through a flow meter to measure its volume and where it showed that more oil was separated than injected.

Finally, there were some other minor problems related to the rig which may have contributed to uncertainties in the measurements. For example, the rotational speed of the electrical motor was difficult to keep constant as it varied +/- 50 revolutions per minute for a certain input.

As was evident from the separator test results, there is still room for improvement regarding the performance of the oil separator. Primarily, the separator needs to be tested at a larger interval of operating points regarding volumetric air- and oil flow, temperatures, pressures and pressure ratios. It is known that the oil has highly temperature dependent characteristics, and that the volume of oil and air greatly affects the separation capabilities. In the end, the concept that showed the greatest potential from the tests conducted was the simple cylindrical container with a low-positioned inlet, schematically shown in figure 6.1. The addition of baffles or flow conditioners could help with performance over a larger flow rate interval. The inner container measures 80 mm in diameter and 150 mm in height.

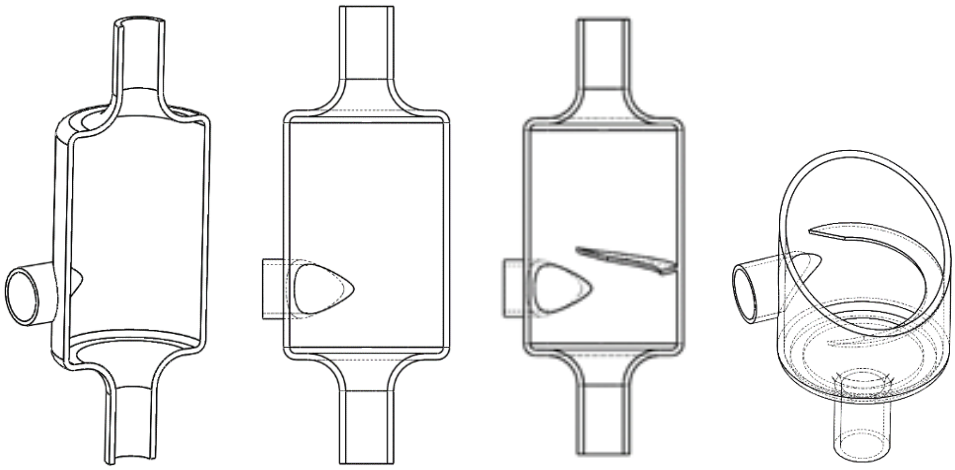

Figure 6.1: Possible layout of separator concepts.

6.3.2 Deaeration device

Due to the lack of tangible results, the following improvement suggestions will be based upon earlier reasoning regarding the deaeration mechanisms. It seems that a lot of the aeration problems can be adequately solved by simply having a reasonably-sized reservoir of oil with an additional insert to promote an evenly dispersed velocity gradient over the cross-section of the reservoir. As could be shown in figure 3.9 under heading 4.2.2, there is a theoretical threshold at a tank diameter of 6 to 7 centimetres when significantly smaller bubbles can be eliminated by slowing down the flow of oil in the opposite direction of the buoyant force. It is therefore concluded that a larger cross section area is very beneficial combined with an attempt at obtaining a thinner layer of oil before it reaches the reservoir. The proposed oil reservoir, as presented in figure 6.2, therefore features a double helix geometry with a riffled surface to increase the surface area on which the oil will pass before entering the main reservoir chamber.

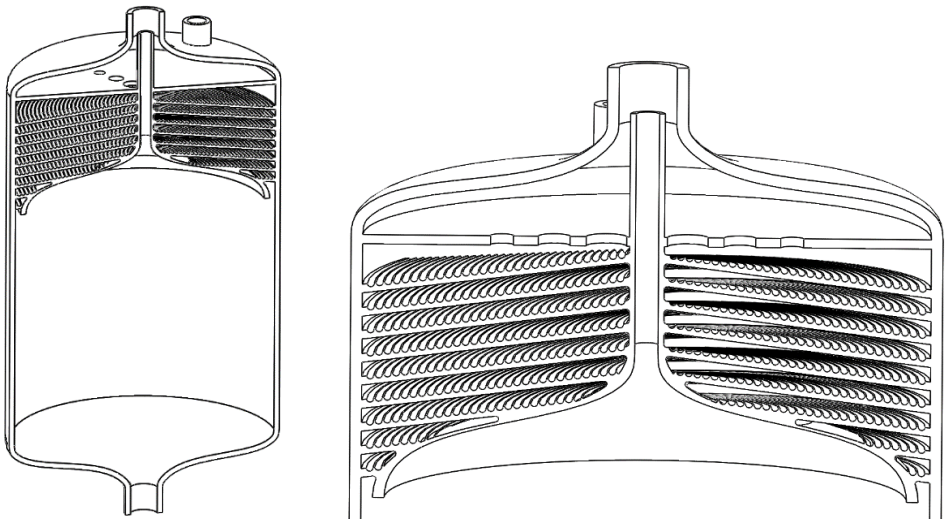

Figure 6.2: Possible concept of deaerator/oil reservoir.

7 Summary and conclusion

The objective of this thesis work was to develop the oil separation- and deaeration systems. The main approach to this was first to conduct research regarding the subject of separating a liquid and gas phase and find concepts that could be applied to this problem. After deciding which concepts to investigate further, it was investigated how these concepts could be designed, manufactured, tested and evaluated.

In the end, no conclusion could be reached as to whether the deaeration concepts gave any improvement regarding the aeration of the oil. Suggestions upon how to proceed with the problem was presented and a schematic design suggestion was proposed.

Separator results showed a clear performance difference between the concepts tested, and that the separation efficiency had a clear correlation to the volumetric air flow. From the results and data gathered, a separator concept could be proposed for further investigation.

8 References

1. Stanton, Donald W., *Systematic Development of Highly Efficient and Clean Engines to Meet Future Commercial Vehicle Greenhouse Gas Regulations*, SAE International, 2008
2. Mahle, https://www.mahle.com/en/products-and-services/commercial-vehicles/air-management/ (Retrieved 10-01-2020)
3. University of Calgary, https://energyeducation.ca/encyclopedia/Cyclone_separator, (retrieved 06-03-2020)
4. Kyldelar AB, http://kyldelar.se/Produkter/Armaturer/Oljeavskiljare/Oljeavskiljare_TURBOIL1503S?id=405601 (retrieved 06-03-2020)
5. Sayako SAKAMA, Yutaka TANAKA, Hiroyuki GOTO, *Mathematical model for bulk modulus of hydraulic oil containing air bubbles*, The Japan Society of Mechanical Engineers, 2015
6. Wikipedia, Coalescence, https://en.wikipedia.org/wiki/Coalescence_(physics), (retrieved 06-03-2020)
7. Stefan Schmidt, Hugh M. Blackburn, Murray Rudman, Ilija Sutalo, *Simulation of turbulent flow in a cyclonic separator*, CSIRO Manufacturing and Infrastructure Technology Australia, 2003
8. Wikipedia, Cyclonic separation, https://en.wikipedia.org/wiki/Cyclonic_separation (Retrieved 15-01-2020)
9. G. Ramachandran , David Leith , John Dirgo & Henry Feldman (1991) *Cyclone Optimization Based on a New Empirical Model for Pressure Drop, Aerosol Science and Technology*, 15:2, 135-148, DOI: 10.1080/02786829108959520
10. Selami Demir, *A practical model for estimating pressure drop in cyclone separators: An experimental study*, Yildiz Technical University, 2014
11. John Dirgo & David Leith (1985) *Cyclone Collection Efficiency: Comparison of Experimental Results with Theoretical Predictions*,

Aerosol Science and Technology, 4:4, 401-415, DOI: 10.1080/02786828508959066
12. D. F. Young, B. R. Munson, T. H. Okiishi, W. W. Huebsch, *Introduction to Fluid Mechanics*, John Wiley & sons, Inc.
13. Petri Sjoholm, Derek B. Ingham, Matti Lehtimaki, Leena Perttu-Roiha, Howard Goodfellow, Heikki Torvela, *Industrial ventilation design guidebook (Chapter 13) Gas cleaning technology, 2001*
14. https://en.wikipedia.org/wiki/Henry%27s_law?fbclid=IwAR3VL16sNEMxhSCumaRrCgCyVBOR3ivMNN_m84M4T91cVuh8FBGyxGwhe0Q, (Retrieved 09-03-2020)
15. *Dynamics of an initially spherical bubble rising in quiescent liquid*, M. Kumar Tripathi , K. Chandra Sahu & R. Govindarajan, 2014
16. https://www.machinerylubrication.com/Read/376/surface-tension-test, (Retrieved 09-03-2020)
17. https://www.cfd-online.com/Wiki/Turbulence_length_scale, (Retrieved 08-03-2020)
18. Zhu Zhiping, Na Yongjie, Lu Qinggang, *Pressure Drop in Cyclone Separator at High Pressure*, Journal of Thermal Science Vol.17, No.3 (2008) 275−280, DOI: 10.1007/s11630-008-0275-7
19. Hineiti, Naser,. Guessous, Laila. *Numerical Investigation of Transient Flow Effects on the Separation Parameters of a Reverse Flow Type Cyclone Particle Separator*, Oakland University, 2008

9 Appendix 1 - Drawings of prototype housing and flanges

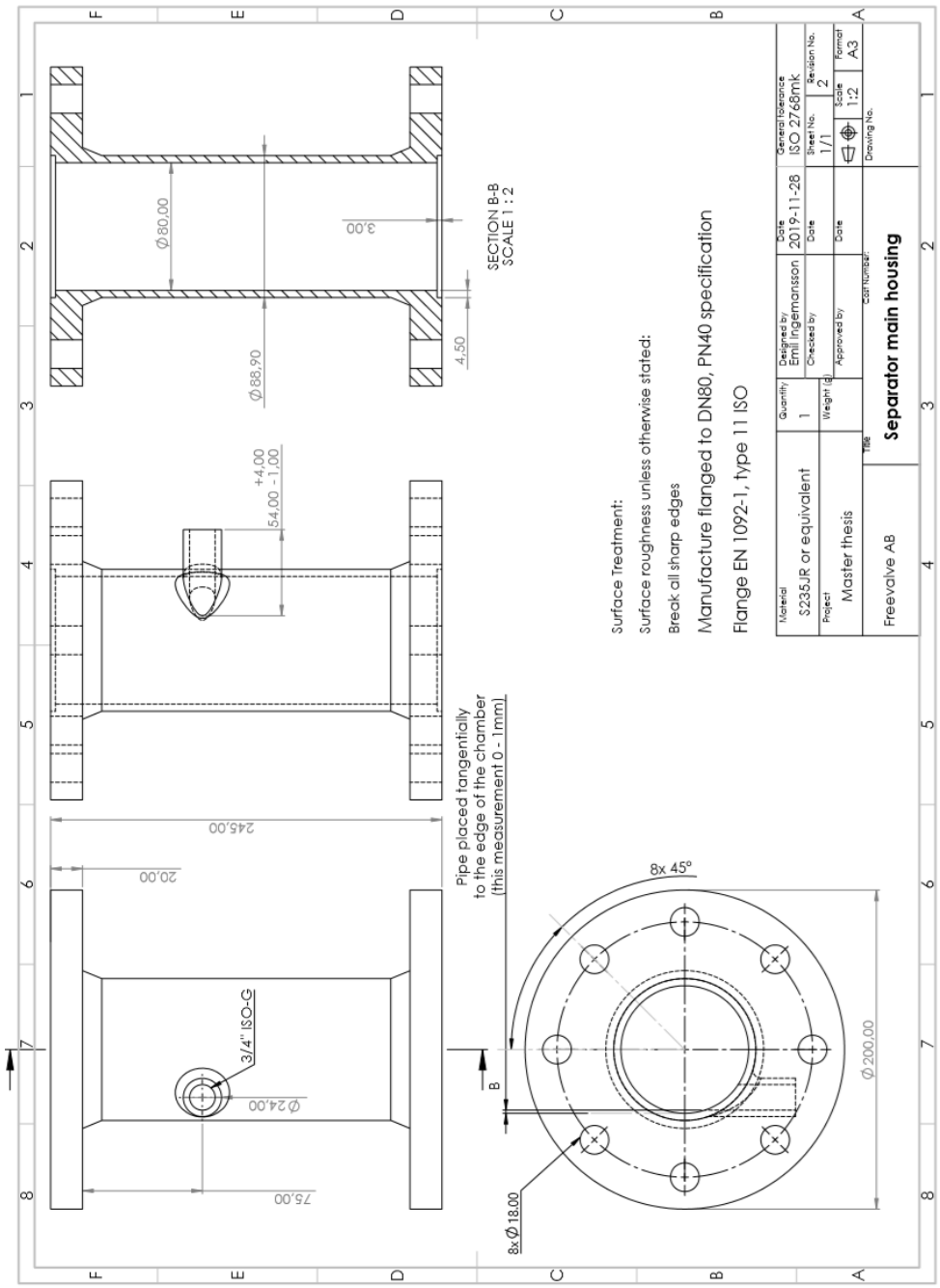

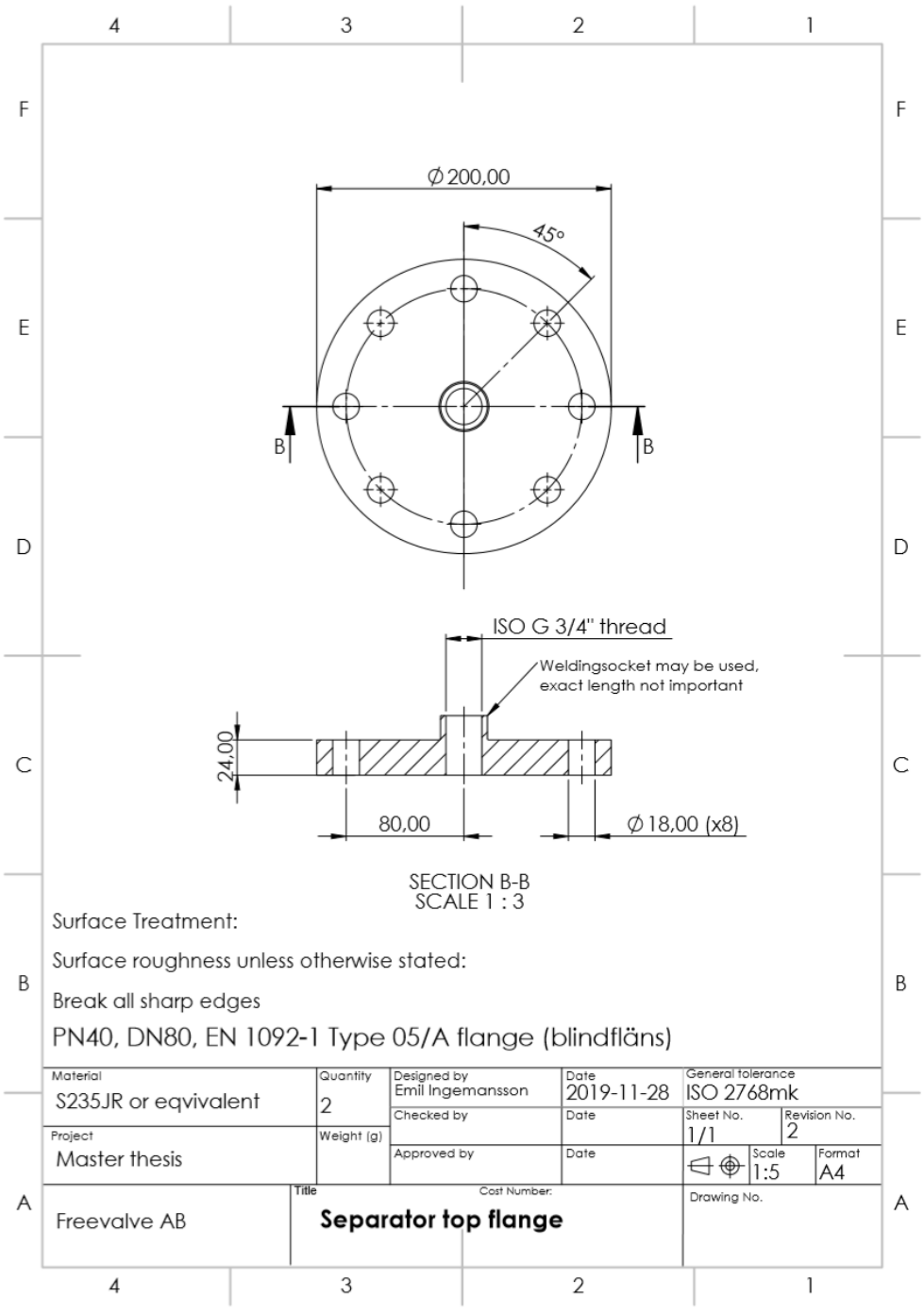
Ø 200,00
45°
B
B
ISO G 3/4" thread
Weldingsocket may be used,
exact length not important
24,00
80,00
Ø 18,00 (x8)
SECTION B-B
SCALE 1 : 3
Surface Treatment:
Surface roughness unless otherwise stated:
Break all sharp edges
PN40, DN80, EN 1092-1 Type 05/A flange (blindfläns)
Material
S235JR or eqvivalent
Quantity
2
Designed by
Emil Ingemansson
Date
2019-11-28
General tolerance
ISO 2768mk
Checked by
Date
Sheet No.
1/1
Revision No.
2
Project
Master thesis
Weight (g)
Approved by
Date
Scale
1:5
Format
A4
Freevalve AB
Title
Separator top flange
Cost Number:
Drawing No.

10 Appendix 2 - Thermal properties of Mobil Rarus SHC 1026

Mobil Rarus SHC 1026

Data has been calculated based on typical properties and do not constitute a specification.

Temperature	Kinematic viscosity	Density	**Specific heat capacity**	Thermal conductivity	Heat capacity per vol.
[°C]	[cSt]	[kg/m3]	[kJ/(kg.K)]	[W/(m.K)]	[kJ/L.K]
0	709,8	863,8	1,988	0,1426	1,72
10	343,5	858,6	2,025	0,1416	1,74
20	183,8	853,4	2,062	0,1405	1,76
30	106,8	848,4	2,098	0,1395	1,78
40	66,6	843,3	2,135	0,1384	1,80
50	44,0	838,4	2,172	0,1373	1,82
60	30,5	833,5	2,208	0,1363	1,84
70	22,1	828,7	2,245	0,1352	1,86
80	16,5	823,9	2,282	0,1341	1,88
90	12,8	819,1	2,318	0,1331	1,90
100	10,1	814,5	2,355	0,1320	1,92
110	8,2	809,8	2,391	0,1309	1,94
120	6,7	805,3	2,428	0,1299	1,96
130	5,7	800,7	2,465	0,1288	1,97
140	4,8	796,3	2,501	0,1278	1,99
150	4,2	791,9	2,538	0,1267	2,01
160	3,6	787,5	2,575	0,1256	2,03
170	3,2	783,2	2,611	0,1246	2,05
180	2,8	778,9	2,648	0,1235	2,06
190	2,5	774,7	2,685	0,1224	2,08
200	2,3	770,5	2,721	0,1214	2,10

11 Appendix 3 - Mobil Rarus SHC 1026 Product datasheet

Mobil

Mobil Rarus SHC™ 1020-serien

Mobil Industrial , Sweden

Luftkompressorolja

Produktbeskrivning

Mobil Rarus SHC™ 1020-serien är en serie av högkvalitativa oljor som främst är avsedda för smörjning av rotationsluftkompressorer av skruv- och vingtyp vilka utsätts för hårda belastningar. De är särskilt lämpade för påfrestande driftsförhållanden där mineraloljebaserade produkter inte uppfyller kraven, såsom i tunga tillämpningar med höga kompressionstemperaturer, eller i fall där förlängda oljebytesintervall är önskvärda. De är tillverkade av vaxfria, syntetiska kolväteoljor och ett högteknologiskt additivsystem som ger mycket hög beständighet mot oxidation och termisk nedbrytning långt utöver vad mineraloljebaserade luftkompressoroljor förmår. De ger enastående utrustningsskydd och pålitlighet för kompressorer som arbetar under förhållanden där andra luftkompressoroljor inte klarar kraven. Mobil Rarus SHC 1020-serien ger utmärkt slitageskydd och enastående beständighet mot oxidation och termisk nedbrytning, klart över vad som presteras av mineraloljor. Deras unika formulering ger möjlighet att sänka underhållskostnaderna genom en minskning av maskinproblemen och avlagringar och rester. Deras höga viskositetsindex säkerställer effektiv smörjning vid höga temperature.

Smörjmedlen i Mobil Rarus SHC 1020-serien minskar avsevärt risken för brand och explosioner, jämfört med mineraloljebaserade produkter. De uppvisar en praktiskt taget total avsaknad av avlagringar samt höga autogena antändningstemperaturer, vilket förbättrar både prestandan och säkerheten. Deras exceptionella vattenseparationsförmåga minskar problemen med emulsionsbildning på koalescens- och filteranordningar, vilket sänker behovet av frekvent underhåll.

Egenskaper och Fördelar

Användning av oljorna i Mobil Rarus SHC 1020-serien kan leda till renare kompressorer och mindre avlagringar jämfört med konventionella mineraloljor, vilket resulterar i längre driftsperioder mellan underhållsintervallen. Oljornas utmärkta oxidations- och värmestabilitet möjliggör säkert förlängda användningstider samtidigt som bildningen av slam och avlagringar kontrolleras. Dessa oljor erbjuder dessutom enastående slitage- och korrosionsskydd, vilket ökar utrustningens livslängd och prestanda.

Egenskaper	Fördelar
Högpresterande, syntetiska basoljor	Brett temperaturområde Väsentligt högre prestanda än mineraloljor Förbättrad säkerhet Förlängda användningstider
Enastående värme- och oxidationsstabilitet	Minskade koksavlagringar Längre användningstid för oljan Förlängd filterlivslängd Lägre underhållskostnader
Hög lastbärande förmåga	Minskat slitage på lager och växlar
Utmärkt vattenseparationsförmåga	Mindre transport av partiklar till retur Minskad slambildning i vevhus och returledningar Minskad blockering av grenrör samt av mellan- och efterkylare Mindre risk för emulsionsbildning
Effektivt rost- och korrosionsskydd	Förbättrat skydd för inre kompressorkomponenter

Användningsområden

Oljorna i Mobil Rarus SHC 1020-serien är främst avsedda för rotationskompressorer av skruv- eller vingtyp. De är särskilt effektiva för kontinuerlig högtemperaturdrift med temperaturer upp till 200 °C. Oljorna i Rarus SHC 1020-serien rekommenderas för enheter som redan råkat ut för alltför kraftig oljenedbrytning, dåliga ventilprestanda eller avlagringsbildning. De är kompatibla med alla metaller som används i kompressorkonstruktion och med konventionella mineraloljebaserade luftkompressoroljor, dock kommer blandning med andra oljor att reducera deras totala prestanda.

Oljorna i Mobil Rarus SHC 1020-serien rekommenderas inte för luftkompressorer som används i andningsluftapplikationer. Produkterna får inte heller användas i kompressorer med en utloppstemperatur överstigande produktens flampunkt.

Följande typer av kompressorapplikationer har uppvisat förträffliga prestanda med oljorna i Mobil Rarus SHC 1020-serien:

- Rekommenderas främst för roterande luftkompressorer av skruv- och vingtyp
- Mycket effektiva i skruvkompressorer med oljekylning
- Enheter som arbetar under krävande förhållanden
- Flerstegskompressorer där det tidigare varit problem med oljenedbrytning orsakad av mineraloljebaserade produkter
- Kompressorsystem med kritiska växlar och lager
- Kompressorer som används i stationära och mobila tillämpningar

Typiska egenskaper

Mobil Rarus SHC 1020-serien	Mobil Rarus SHC 1024	Mobil Rarus SHC 1025	Mobil Rarus SHC 1026
ISO VG -klass	32	46	68
Viskositet, ASTM D 445			
cSt @ 40°C	31.5	44	66.6
cSt @ 100°C	5.7	7.2	10.1
Viskositetsindex, ASTM D 2270 , min	127	131	136
Kopparkorrosion, ASTM D130, 24 tim @ 100°C	1B	2A	1B
Rostegenskaper Proc A, ASTM D 665	Godk	Godk	Godk
Lägsta flyttemp, ASTM D 97, °C, max	-48	-45	-45
Flampunkt, °C, ASTM D 92	245	246	246
Relativ densitet 15°C/15°C, ASTM D 1298	0.846	0.849	0.856

Hälsa och säkerhet

På underlag av tillgänglig information förväntas inte denna produkt ha någon hälsovådlig inverkan när den används för avsedd applikation, och när rekommendationerna i säkerhetsdatabladet följs. Säkerhetsdatabladen kan fås på begäran via ditt lokala säljkontor eller via Internet. Denna produkt bör inte användas för andra ändamål än den är avsedd för. Se till att skona miljön när produkten bortskaffas.

11-2019
ExxonMobil Sverige AB
Box 1035 (Fabriksgatan 7)
SE 405 22 Göteborg

+46 31 638200
http://www.exxonmobil.com